Single-Tryptophan Mutants of Monomeric Tryptophan Repressor: Optical Spectroscopy Reveals Nonnative Structure in a Model for an Early Folding Intermediate†

Xiao Shao‡ and C. Robert Matthews*

Department of Chemistry and Center for Biomolecular Structure and Function, The Pennsylvania State University, University Park, Pennsylvania 16802

Received December 29, 1997; Revised Manuscript Received March 27, 1998

ABSTRACT: A monomeric version of the dimeric tryptophan repressor from *Escherichia coli*, L39E TR, has previously been shown to resemble a transient intermediate that appears in the first few milliseconds of folding [Shao, X., Hensley, P., and Matthews, C. R. (1997) *Biochemistry 36*, 9941−9949]. In the present study, the optical properties of the two intrinsic tryptophans were used to compare the structure and dynamics of the monomeric form with those of the native, dimeric form. The urea-induced unfolding equilibria of Trp19/L39E TR (Trp99 replaced with Phe) and Trp99/L39E TR (Trp19 replaced with Phe) mutants were monitored by circular dichroism and fluorescence spectroscopies at pH 7.6 and 25 °C. Coincident normalized transitions show that the urea denaturation process for each single-tryptophan mutant follows a two-state model involving monomeric native and unfolded forms. The free energies at standard state in the absence of denaturant for Trp19/L39E TR and Trp99/L39E TR are less than that for L39E TR, indicating that both tryptophans are involved in stabilizing the monomer. Fluorescence and near-UV circular dichroism spectroscopies indicate that the tryptophan side chains in monomeric Trp19/L39E TR and Trp99/L39E TR occupy hydrophobic, well-structured environments that are distinctively different from those found in their dimeric counterparts. Acrylamide quenching experiments show that both Trp19 and Trp99 are partially exposed to solvent in the native state, with Trp99 having a slightly greater degree of exposure. Measurements of the steady-state anisotropies of Trp19/L39E and Trp99/L39E TR demonstrate that the motions of both tryptophan side chains are restricted in the folded conformation. On the basis of these data, it can be concluded that this monomeric form of the tryptophan repressor adopts a well-folded, stable conformation with nonnative tertiary structure. When combined with previous results, the current findings demonstrate that the development of higher order structure during the folding of this intertwined dimer does not follow a simple hierarchical model.

A common strategy for unraveling the relationship between the amino acid sequence of a protein and its three-dimensional structure is to probe the structure and stability of partially folded forms that appear during the folding reaction (*1*−*4*). Stopped-flow spectroscopic and hydrogen exchange NMR techniques have been very useful to this approach (*5*−*9*). Nativelike secondary structure has been observed to form at an early stage of the folding reaction for a number of proteins, including α-lactalbumin (*10*, *11*), lysozyme (*12*, *13*), cytochrome *c* (*14*, *15*), apomyoglobin (*16*, *17*), dihydrofolate reductase (*18*), and ribonuclease H (*19*).

The presence of nativelike intermediates supports a hierarchical folding model which begins with the formation of individual elements of secondary structure (*3*, *20*), the adhesion of these elements to form subdomains (*21*), and the association/annealing of these subdomains to form the native conformation. These events are likely to occur in the context of a collapsed polypeptide whose formation is driven by the hydrophobic effect (*22*).

By contrast, a helical intermediate appears during the folding of β-lactoglobulin, whose native structure contains primarily β-strands (*11*, *23*, *24*). A nonnative monomeric intermediate has been proposed for the folding of the dimeric DNA binding domain of the human papillomavirus E2 protein (*25*). Transient, nonnative interactions have also been observed in the early folding intermediates of the *Escherichia coli* tryptophan synthase β_2 subunit (*26*) and TEM-1 B-lactamase (*27*). These results suggest that a hierarchical folding model may not pertain to all proteins.

The tryptophan repressor from *E. coli* (Figure 1) (*28*) is another potential candidate for a nonnative folding intermediate. Each subunit of this homodimer consists of six helices, A−F. The first three helices from each subunit form a hydrophobic dimeric interface, largely dominated by inter-subunit nonpolar interactions. Helices D and E form the DNA reading heads, and helix F folds against that part of the core contributed by the other subunit.

In a previous study of dimeric, wild-type tryptophan repressor (WT TR),[1] a stable monomeric intermediate was found to be highly populated in a burst phase folding reaction

† This work was supported by the National Institutes of Health through Grant GM 54836 to C.R.M.

* Author to whom correspondence should be addressed.

‡ Present address: Department of Chemistry, Rutgers University, Piscataway, NJ 08855-0939.

S0006-2960(97)03171-1 CCC: $15.00
Published on Web 05/07/1998

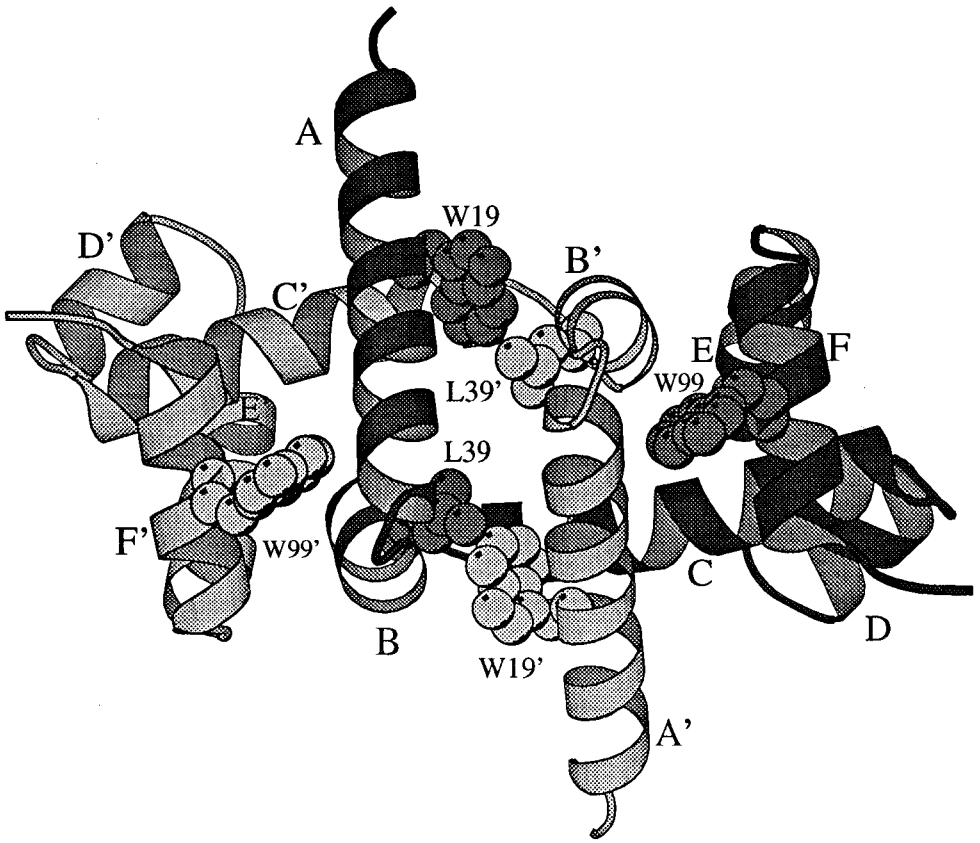

FIGURE 1: Ribbon diagram of the dimeric tryptophan repressor (*28*), in which the individual subunits are shown in dark and light shading, respectively, and residues Trp19, Trp99, and Leu39 are highlighted. The six helices in each monomer, A through F, are labeled. This figure was generated using Molscript v1.4 (*49*).

(*29*). The complex, intertwined topology observed in the dimeric protein implies that a monomeric folding intermediate is very unlikely to adopt the conformation observed in the dimer. The monomeric form would be more likely to collapse into a compact, nonnativelike structure that replaces intermolecular hydrophobic surfaces with intramolecular surfaces.

L39E TR, in which a leucine residue buried at the dimer interface is replaced by a glutamic acid, is a well-folded, thermodynamically stable monomeric protein at micromolar concentrations (*30*). Spectroscopic, thermodynamic, and kinetic studies demonstrated that this monomeric trp repressor is very similar to the burst phase intermediate in the refolding of wild-type TR. The favorable optical properties of tryptophan make it an ideal probe to compare structural and dynamic features of monomeric and dimeric TR. Trp19 is located in helix A and is buried in the hydrophobic core of the dimer. Trp99 is located in helix F and is packed against the core (Figure 1). By constructing two monomeric single-tryptophan mutants, Trp19/L39E TR and Trp99/L39E TR, it was possible to examine the structural and dynamic properties of the sole remaining tryptophan.

Comparison of the results with those from the corresponding single-tryptophan mutants of dimeric TR shows that the monomeric repressor can adopt a well-folded conformation whose tryptophan side chains occupy environments that are distinctly different from those in the dimeric form. The existence of an alternative, nonnative conformer in these models of an early intermediate in the folding of the tryptophan repressor strongly suggests that the hierarchical model does not apply to this intertwined dimeric protein.

MATERIALS AND METHODS

Chemicals. Ultrapure urea was purchased from ICN Biomedicals, Inc. (Costa Mesa, CA) and used without further purification. All other chemicals were reagent grade. The thoroughly degassed buffer used in all experiments contained 10 mM sodium phosphate and 0.1 mM Na_2EDTA at pH 7.6.

Mutagenesis and Protein Purification. Trp19/L39E TR and Trp99/L39E TR were constructed using PCR techniques (*31*, *32*) to introduce the TTT codon at the desired positions in the pT_7RUC plasmid which contained the L39E TR gene (*30*). The plasmids containing the mutations were then transformed into *E. coli* strain JM109(DE3) for expression.

[1] Abbreviations: CD, circular dichroism; COM, center of mass wavelength for fluorescence emission; FL, fluorescence; L39E TR, the tryptophan aporepressor mutant in which leucine at position 39 is replaced by glutamic acid; IPTG, isopropyl-β-D-thiogalactopyranoside; Na_2EDTA, ethylenediaminetetraacetic acid, disodium salt; $NaDodSO_4$, sodium dodecyl sulfate; MRE, mean residue ellipticity; SSA, steady-state anisotropy; SVD, singular value decomposition; Trp19/L39E TR, the monomeric single-tryptophan trp aporepressor mutant in which tryptophan at position 99 and leucine at position 39 are replaced by phenylalanine and glutamic acid, respectively; Trp99/L39E TR, the monomeric single-tryptophan trp aporepressor mutant in which tryptophan at position 19 and leucine at position 39 are replaced by phenylalanine and glutamic acid, respectively; W99F TR, single-tryptophan mutant of trp repressor with phenylalanine substituted for tryptophan at position 99 in both subunits and the wild-type tryptophan at position 19; W19F TR, single-tryptophan mutant of trp repressor with phenylalanine substituted for tryptophan at position 19 in both subunits and the wild-type tryptophan at position 99; WT TR, dimeric wild-type trp aporepressor.

The mutant proteins were overproduced as inclusion bodies following induction by IPTG.

The purification of these two mutant proteins followed procedures described previously (*30*) with one exception. Phenyl sepharose high-performance (HP) resin (Pharmacia, Uppsala, Sweden) was used to remove most of the contaminating proteins which were still present after the ion-exchange column. This hydrophobic column was equilibrated with 20 mM potassium phosphate buffer, pH 7.6, containing 10% (weight/volume) ammonium sulfate. After the protein solution was loaded on the column, undesired proteins were removed by running the same buffer overnight at 4 °C. The mutant protein was then eluted by a gradient of phosphate buffer containing 0.4−0 M ammonium sulfate at a flow rate of 0.5−1 mL m^{-1}. The purity of the final protein product after treatment on the hydrophobic column was about 80−90% as judged by $NaDodSO_4$ polyacrylamide gel electrophoresis. A further step of size exclusion chromatography on G-50 resin (Pharmacia) removed the remaining contaminants and yielded a single band on a $NaDodSO_4$ polyacrylamide gel. The purified protein was stored as a 70% ammonium sulfate precipitate at 4 °C and dialyzed against sodium phosphate buffer (10 mM sodium phosphate and 0.1 mM Na_2EDTA, pH 7.6) prior to use.

The extinction coefficients of both Trp19/L39E TR and Trp99/L39E TR were determined to be 8.3×10^3 M^{-1} cm^{-1} at 280 nm, according to the method of Gill and von Hippel (*33*).

Spectroscopic Methods. CD spectra were collected on an AVIV Associates model 62 DS circular dichroism spectrometer; a detailed description of the procedure can be found elsewhere (*30*). Steady-state fluorescence measurements were collected on an AVIV Associates model ATF 105 spectrofluorometer. Intrinsic tryptophan fluorescence emission spectra were recorded from 310 to 450 nm with excitation at 295 nm.

The acrylamide quenching experiment was performed with an automated Hamilton Microlab 540B titrating system linked to the ATF 105 fluorometer. The titrators were used to systematically adjust the acrylamide concentration from 0 to 0.50 M by using a preset macro program. Fluorescence intensities at 340 nm were collected with a 4 nm excitation and a 5 nm emission bandwidth. Fluorescence quenching data were then analyzed according to the Stern−Volmer equation:

$$F_o/F = (1 + K_{sv}[Q]) \exp(V[Q]) \quad (1)$$

where F_o and F are the fluorescence intensities in the absence and presence of acrylamide, K_{sv} and V are the dynamic and static quenching constants, and [Q] is the concentration of acrylamide. The term, exp(V[Q]), reflects static quenching by acrylamide.

The anisotropy data were collected on an AVIV ATF 105 fluorometer with Glan−Taylor excitation/emission polarizers installed. The automated titrators were used to adjust the urea concentration from 0 to 8 M. The parallel and perpendicular polarized intensities and the G factors at 340 nm were recorded at each urea concentration. The urea concentrations were confirmed by measuring the refractive index of the two initial stock buffers, which were 0 and 8 M urea, and the final solution in the cuvette after the experiment was finished. The final refractive index value was consistent with the expected value, confirming the reliability of the automated titrators.

Steady-state anisotropy data were calculated based on the following equations:

$$S = I_{||} + 2GI_{\perp} \quad (2a)$$

$$r = \frac{I_{||} - GI_{\perp}}{I_{||} + 2GI_{\perp}} \quad (2b)$$

where $I_{||}$ and $I_{\perp}$ are the emission intensities collected at polarization parallel or perpendicular to the polarization of the exciting light. S is the total fluorescence intensity, r is the steady-state anisotropy, and G is a factor accounting for the bias of the detection system for vertically versus horizontally polarized light. All fluorescence spectra were corrected for solvent background.

Analytical Ultracentrifugation. Equilibrium ultracentrifuge data were collected on a Beckman XL-I analytical ultracentrifuge, and the data were analyzed by previously described methods (*30*).

Fitting of Equilibrium Unfolding Data. The equilibrium unfolding data were fit to a two-state model:

$$N \overset{K}{\rightleftharpoons} U$$

where N is the native monomer, U is the unfolded monomer, and K = [U]/[N]. CD data at 222 nm were corrected to mean residue ellipticity and analyzed by procedures that have been described previously (*30*). The fluorescence emission data were analyzed by both center of mass wavelength (*30*) and SVD analysis. The COM analysis was used to provide a simple description of the optical properties of the mutant proteins. The COM analysis can bias thermodynamic parameters when the integrated intensities of the constituent spectra are not identical. Thus, the SVD analysis was used to extract thermodynamic parameters.

With the SVD algorithm (*34*), the fluorescence emission spectra were decomposed into spectral and urea-dependent basis vectors. The basis spectra that were nonrandom were chosen to represent the data. In addition to visual inspection, three criteria were used in determining the number of basis vectors to include: (1) the singular values (or weights) from the SVD, (2) the autocorrelation of the U-vectors, and (3) the autocorrelation of the V-vectors. This analysis gives the minimum number of spectrally distinguishable components in the data set (*35*). The orthonormal basis vectors, however, do not necessarily represent the actual spectra of the molecular species (*35*). The basis vectors representing the urea dependence were fit to a monomeric two-state equilibrium model (*36*) by a global analysis (*37*) that links the free energy difference in the absence of denaturant, $\Delta G°(H_2O)$, and the sensitivity of the unfolding transition to urea, the m value, across the basis vectors. Thus, for n basis vectors, $4n + 2$ parameters are required. The in-house global analysis package, Savuka 5.1, was used to fit the CD and fluorescence data.

Steady-state anisotropy data were fit to a two-state equilibrium unfolding model. The steady-state intensity, S, and steady-state anisotropy, r, can be written as

$$S = f_N S_N + f_U S_U \quad (3)$$

$$r = \frac{f_N S_N}{S} r_N + \frac{f_U S_U}{S} r_U \quad (4)$$

in which the subscripts N and U denote native and unfolded species, f_N and f_U are molar fractions ($f_N + f_U = 1$), S_N and S_U are the intrinsic fluorescence properties including the quantum yield and extinction coefficient, and r_N and r_U are the anisotropy values, respectively. S_N, S_U, r_N, and r_U were assumed to depend linearly on denaturant concentration according to the following equations:

$$S_N = S_N(H_2O) + a_N[\text{urea}] \quad (5a)$$

$$S_U = S_U(H_2O) + a_U[\text{urea}] \quad (5b)$$

$$r_N = r_N(H_2O) + b_N[\text{urea}] \quad (6a)$$

$$r_U = r_U(H_2O) + b_U[\text{urea}] \quad (6b)$$

where a_N, a_U, b_N, and b_U are the slopes of the pre- and post-transition regions for the fluorescence intensities and anisotropy values of the native and unfolded forms, respectively (*38*). The in-house software package, Savuka 5.1, was used to globally fit the parallel and perpendicular intensities to the two-state equilibrium unfolding model to obtain the free energy difference in the absence of denaturant, $\Delta G°(H_2O)$, and the sensitivity of the unfolding transition to urea, *m*.

RESULTS

Monomer/Dimer Equilibria for Trp19/L39E TR and Trp99/L39E TR. Similar to L39E TR (*30*), equilibrium sedimentation experiments revealed that the single-tryptophan mutants, Trp19/L39E TR and Trp99/L39E TR, are also in monomer/dimer equilibrium under native conditions (data not shown). The dissociation constants of Trp19/L39E TR and Trp99/L39E TR are $(0.71 \pm 0.04) \times 10^{-4}$ and $(1.23 \pm 0.09) \times 10^{-4}$ M, respectively, comparable to that of L39E TR, $(1.11 \pm 0.04) \times 10^{-4}$ M. To emphasize the properties of the monomeric form, the protein concentration was generally kept below 5 μM, where the monomeric form comprised greater than 90% of the population.

Spectroscopic Studies of Monomeric Trp19/L39E TR and Trp99/L39E TR. To gain insight into the structural and dynamic properties of these monomeric versions of TR, spectroscopic studies, including far- and near-UV CD, fluorescence intensity, fluorescence quenching, and fluorescence anisotropy experiments, were carried out.

The secondary structures of Trp19/L39E TR and Trp99/L39E TR were monitored by far-UV circular dichroism at 25 °C and pH 7.6. At 0 M urea, the dual minima in ellipticity at ~208 and ~222 nm CD for both mutants demonstrate the presence of α-helices (Figure 2). The mean residue ellipticities of Trp19/L39E TR and Trp99/L39E TR at 222 nm are -14 and -13×10^3 deg cm^2 dmol^{-1}, respectively. These values are essentially identical to that observed in monomeric L39E TR, -14×10^3 deg cm^2 dmol^{-1} (*30*), suggesting that the tryptophan mutations have little effect on secondary structure. When the urea concentration is increased, the decrease in the ellipticities at 222 nm for both mutants reflects the disruption of secondary structure by the denaturant (Figure 2).

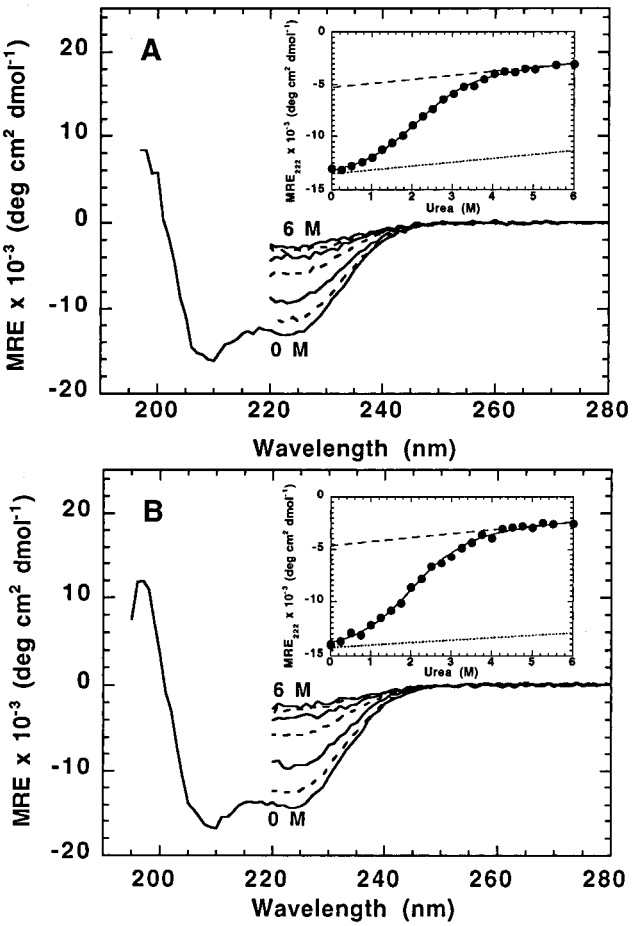

FIGURE 2: The far-UV CD spectra of (A) Trp19/L39E TR and (B) Trp99/L39E TR at different urea concentrations at pH 7.6 and 25 °C. The alternating solid and dashed lines from low to high mean residue ellipticity represent the spectra in 0.0, 1.0, 2.0, 3.0, 4.0, 5.0, and 6.0 M urea. The insets are the mean residue ellipticities of Trp19/L39E and Trp99/L39E at 222 nm as a function of urea. Lines are fits of the data to a two-state equilibrium model (*36*). The dotted and dashed lines represent the urea dependences of the native and unfolded species, respectively. The concentrations of Trp19/L39E TR and Trp99/L39E TR were 2.6 and 2.3 μM, respectively, in a buffer containing 10 mM sodium phosphate and 0.1 mM Na_2EDTA.

The tertiary structure of the single-tryptophan mutants was monitored by steady-state fluorescence spectroscopy. Under native conditions, the spectra for both mutants showed a maximum intensity near 340 nm (Figure 3), indicating that both tryptophans are at least partially buried in hydrophobic environments. As the urea concentration is increased, the decrease in intensity and shift of the spectrum to longer wavelengths for both mutants implies that the remaining tryptophan residue is exposed to the solvent upon unfolding. The spectra at different urea concentrations were also analyzed by calculating the center of mass wavelength. Sigmoidal plots characteristic of cooperative unfolding transitions were observed for both mutant proteins (insets in Figure 3). In the post-transition zone, Trp19/L39E TR exhibits a small linear dependence on denaturant concentration, suggesting that residual structure may persist around Trp19 at high urea concentrations. Comparing the total red shift represented by COM values between the native and unfolded conditions in both mutants (Table 1), the larger

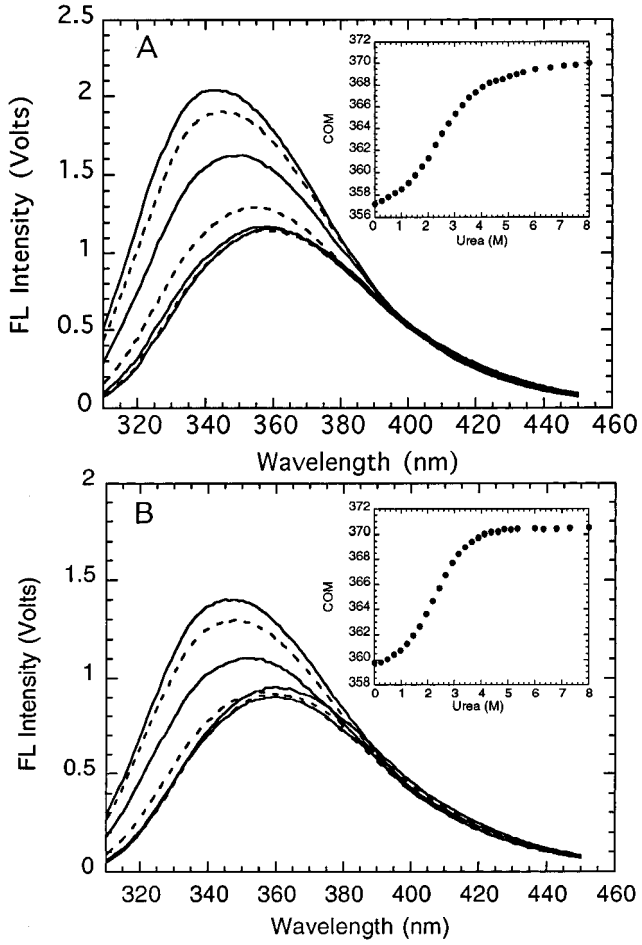

FIGURE 3: The intrinsic tryptophan emission spectra of (A) Trp19/L39E TR and (B) Trp99/L39E TR at different urea concentrations at pH 7.6 and 25 °C. The alternating solid and dashed lines from high to low intensities represent 0.0, 1.0, 2.0, 3.0, 4.0, 5.0, and 6.0 M urea. The insets are the center of mass wavelength (COM) values for Trp19/L39E and Trp99/L39E as a function of urea. The concentrations of Trp19/L39E TR and Trp99/L39E TR were 2.6 and 2.3 μM, respectively. The buffer is described in the caption for Figure 2.

shift observed for Trp19/L39E TR compared to Trp99/L39E TR, 12.8 versus 10.4 nm, suggests that Trp19 may be in a slightly more nonpolar environment in the native state. Neither of the tryptophans in the monomeric form is in an environment as hydrophobic as Trp19 in the dimeric TR (Table 1); however, their environments are comparable to that for Trp99 in the dimeric form.

To further test the tertiary packing around the aromatic chromophores in each mutant, near-UV CD spectra were obtained. At 0 M urea, both tryptophan mutants show distinct signals from 260 to 295 nm; Trp19/L39E TR has negative ellipticities (Figure 4A), and Trp99/L39E TR has positive ellipticities (Figure 4B). As the urea concentration is increased, the negative signals for Trp19/L39E TR and the positive signals for Trp99/L39E TR both decrease to similar, nonzero values. These results demonstrate that specific side chain packing which exists in the native state of both monomeric TR variants is disrupted upon unfolding. The small near-UV CD signals apparent at 6 M urea may reflect spatial constraints on the aromatic side chains that are imposed by the primary structure or by residual tertiary structure.

Table 1: Comparison of the Center of Mass Wavelength Values of Tryptophans in Monomeric and Dimeric TR in Native and Unfolded States[a]

	native state (nm)	unfolded state (nm)	red shift (nm)
monomeric TR			
Trp19/L39E	357.2	370.0	12.8
Trp99/L39E	360.1	370.5	10.4
dimeric TR			
W99F (Trp19)	348.4	370.0	21.6
W19F (Trp99)	355.0	369.5	14.5

[a] The COM values for each protein were calculated from the fluorescence emission spectra collected at 0 (native state) and 8 M (unfolded state) urea concentrations, respectively. Conditions: 10 mM sodium phosphate, 0.1 mM Na_2EDTA, pH 7.6, and 25 °C.

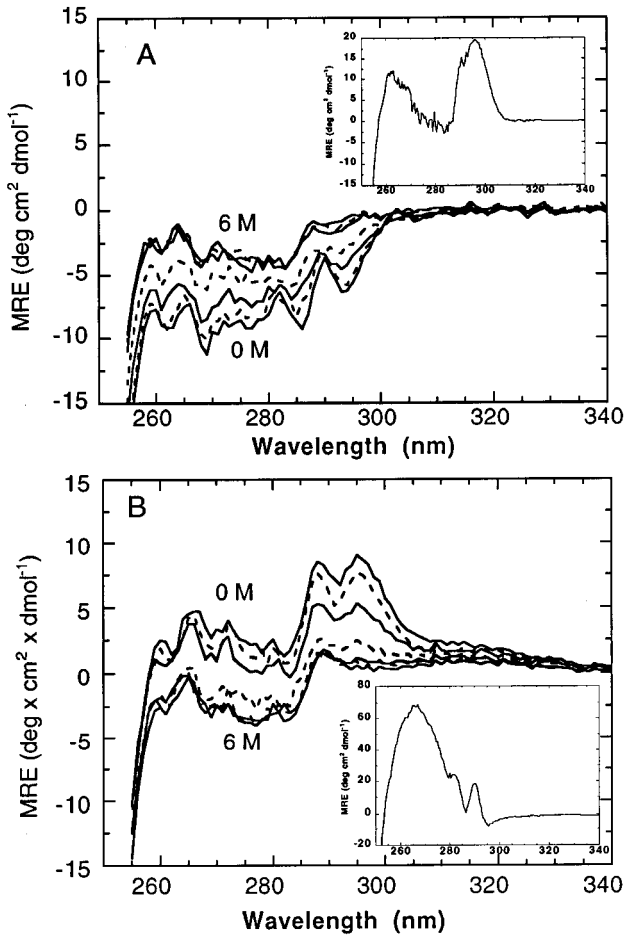

FIGURE 4: The near-UV CD spectra of (A) Trp19/L39E TR and (B) Trp99/L39E TR at different urea concentrations at pH 7.6 and 25 °C. The alternating solid and dashed lines represent the mean residue ellipticity in 0.0, 1.0, 2.0, 3.0, 4.0, 5.0, and 6.0 M urea as indicated. The insets in panels (A) and (B) are the near-UV CD spectra of dimeric W99F TR and W19F TR at 0.0 M urea, respectively. The protein concentrations were 20 μM for both Trp19/L39E TR and Trp99/L39E TR, 14 μM for W99F TR, and 16 μM for W19F TR in terms of monomer. The buffer is described in the caption for Figure 2.

When the near-UV CD spectrum of each monomeric single-tryptophan mutant is compared to the spectrum of the corresponding dimeric single-tryptophan mutant under native conditions (insets in Figure 4), significant differences are apparent in the range from 290 to 300 nm. These data show that the packing around the tryptophan side chain in both

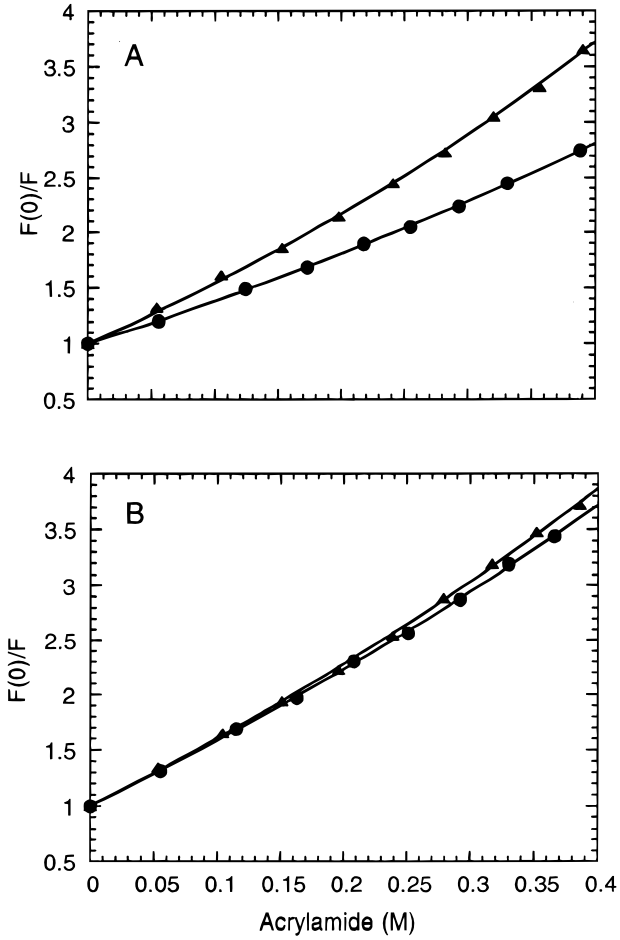

FIGURE 5: Comparison of the effect of acrylamide on the fluorescence intensity of Trp19 and Trp99 in monomeric and dimeric forms of TR at pH 7.6 and 25 °C. (A) The Stern−Volmer plots of Trp19/L39E TR (▲) and W99F TR (●). (B) The Stern−Volmer plots of Trp99/L39E TR (▲) and W19F TR (●). The protein concentration was 2.23 μM for both Trp19/L39E TR and Trp99/L39E TR. The concentrations of W99F and W19F TRs were 3 μM. The buffer is described in the caption for Figure 2.

monomeric TR variants is different than that found in dimeric tryptophan repressor.

To test the accessibility of the tryptophan residues to solvent, fluorescence quenching experiments were carried out. Because quenching agents with a formal charge would be affected by the electric field in the vicinity of each tryptophan, acrylamide, a neutral molecule, was used to quench tryptophan fluorescence. These experiments were performed at 0 and 6 M urea to probe the native and unfolded conformations. The Stern−Volmer plots of Trp19/L39E TR and Trp99/L39E TR are shown in Figure 5, and the results are summarized in Table 2. The upward curvature observed in the plots suggests that both static and dynamic quenching mechanisms are operative. The dynamic quenching constant, K_{sv}, for Trp19/L39E TR under native conditions is 4.17 ± 0.12 M^{-1}. This value is somewhat larger than that for Trp19 in dimeric TR, 2.92 ± 0.10 M^{-1} (see also Eftink et al., ref *39*), but substantially smaller than that observed for this residue in unfolded Trp19/L39E TR, 15.9 ± 0.7 M^{-1}. These results imply that Trp19 must be somewhat more exposed to solvent in folded, monomeric tryptophan repressor than when it is buried at the subunit interface in the dimeric repressor (Figure 1). The K_{sv} for Trp99/L39E TR, 5.13 ± 0.15 M^{-1}, is very similar to the value for Trp99 in dimeric repressor, 5.06 ± 0.15 M^{-1} (Table 2) (*39*), implying comparable solvent exposure. The magnitude of the K_{sv} values in 6 M urea for both Trp19/L39E TR and Trp99/L39E TR indicates that both tryptophans are fully accessible to solvent when the proteins are unfolded (*40*).

Table 2: Stern−Volmer Quenching Constants for Monomeric and Dimeric TRs[a]

protein	urea (M)	K_{SV} (M^{-1})	V (M^{-1})
Trp19/L39E	0	4.17 ± 0.12	0.83 ± 0.04
W99F(dimer)	0	2.92 ± 0.10	0.65 ± 0.05
Trp99/L39E	0	5.13 ± 0.15	0.59 ± 0.05
W19F(dimer)	0	5.06 ± 0.15	0.51 ± 0.06
Trp19/L39E	6	15.9 ± 0.7	0.75 ± 0.21
Trp99/L39E	6	16.2 ± 1.3	0.93 ± 0.36

[a] The samples were excited at 295 nm, and the intensity was monitored at 340 nm. Acrylamide was used as the quencher. The protein concentrations of Trp19/L39E TR and Trp99/L39E TR were both 2.23 μM. The protein concentrations of W99F and W19F were both 6.0 μM in terms of monomer. Conditions: 10 mM sodium phosphate, 0.1 mM Na_2EDTA, pH 7.6, and 25 °C.

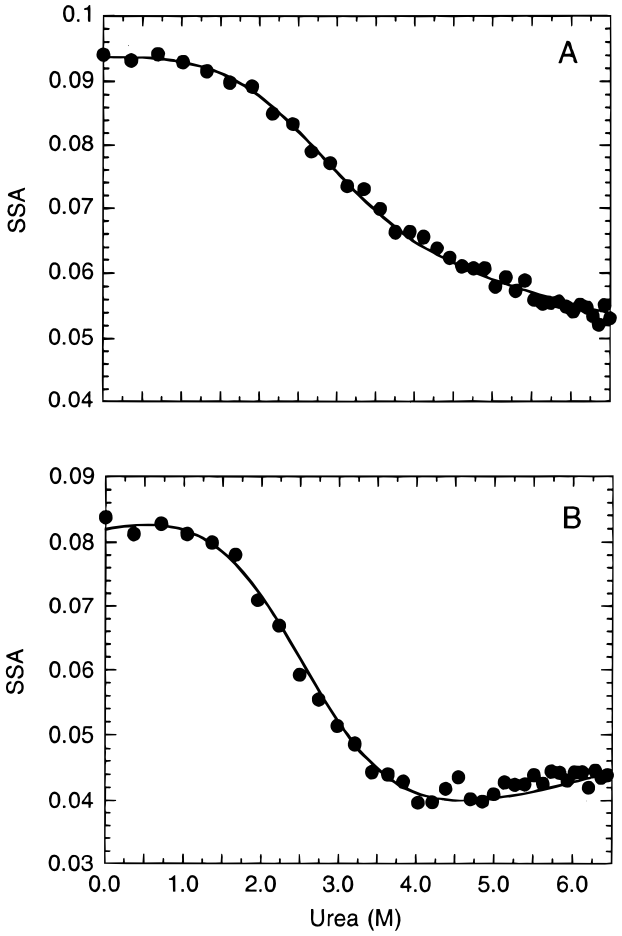

FIGURE 6: The steady-state anisotropy values of (A) Trp19/L39E TR and (B) Trp99/L39E TR as a function of urea at pH 7.6 and 25 °C. The protein concentrations were 2.23 μM for both Trp19/L39E TR and Trp99/L39E TR. The buffer is described in the caption for Figure 2. Lines represent fits of the data to a two-state model as described in Materials and Methods.

The dynamic properties of each tryptophan were explored by measuring the steady-state anisotropy. As shown in Figure 6, the anisotropy of both Trp19/L39E TR and Trp99/L39E TR decreases in a sigmoidal fashion as the urea

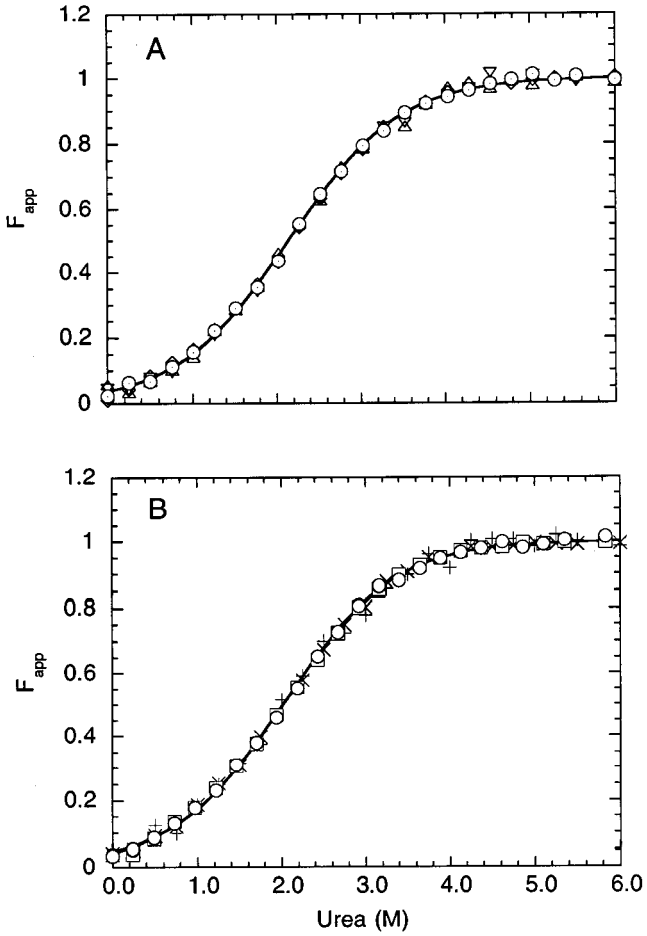

FIGURE 7: The dependence of the apparent fraction of unfolded protein, F_{app}, of (A) Trp19/L39E TR and (B) Trp99/L39E TR on the urea concentration at pH 7.6 and 25 °C as monitored by far-UV CD and tryptophan fluorescence spectroscopies. The data shown in plot A are the mean residue ellipticities at 222 nm at two protein concentrations, 2.6 μM (△) and 14.4 μM (⊙), and the highest weighted component from the SVD analysis of fluorescence emission spectra at two protein concentrations, 2.6 μM (▽) and 14.4 μM (◇). The data shown in the plot B are the mean residue ellipticities at 222 nm at two protein concentrations, 2.3 μM (+) and 12.1 μM (○) and the highest weighted component from the SVD analysis of fluorescence emission spectra at two protein concentrations, 2.3 μM (×) and 12.1 μM (□). The lines represent the combined global fit of the CD and fluorescence data to a two-state model. Based upon the K_d values obtained from ultracentrifugation, the predicted fraction of dimer for either mutant in the absence of denaturant ranges from 6.4 to 24% for Trp19/L39E and from 3.5 to 14% for Trp99/L39E.

concentration is increased. These results indicate that the mobility of both tryptophans increases upon unfolding. The linear decrease in the anisotropy of Trp19/L39E TR above 4 M urea suggests that Trp19 may participate in residual structure present at high denaturant concentration.

Equilibrium Unfolding Studies of Monomeric Trp19/L39E TR and Trp99/L39E TR. To test the cooperativity of the unfolding titration and determine whether the folded forms of Trp19/L39E TR and Trp99/L39E TR behave as distinct thermodynamic states, the equilibrium unfolding transitions of each of the monomeric single-tryptophan mutants were monitored by far-UV CD and tryptophan fluorescence spectroscopic methods at two different protein concentrations and at pH 7.6 and 25 °C (Figure 7). By varying the protein concentration, the possible contribution of the dimeric forms of these mutants to the apparent stability can be examined. Anisotropy values were measured at a single protein concentration.

Table 3: Thermodynamic Parameters for Monomeric Trp19/L39E TR and Trp99/L39E TR[a]

protein	technique	concn (μM)	$\Delta G°(H_2O)$ (kcal mol^{-1})	m (kcal mol^{-1} M^{-1})
Trp19/L39E TR	CD	2.6	1.79 ± 0.34	0.81 ± 0.09
	FL(SVD)[b]	2.6	1.52 ± 0.27	0.74 ± 0.09
	CD	14.4	1.83 ± 0.19	0.83 ± 0.05
	FL(SVD)[b]	14.4	2.01 ± 0.10	0.91 ± 0.03
	global[c]		1.93 ± 0.08	0.90 ± 0.02
	anisotropy	2.23	1.81 ± 0.03	0.86 ± 0.02
Trp99/L39E TR	CD	2.3	1.57 ± 0.35	0.79 ± 0.08
	FL(SVD)[b]	2.3	1.81 ± 0.10	0.91 ± 0.03
	CD	12.1	1.88 ± 0.29	0.88 ± 0.08
	FL(SVD)[b]	12.1	1.79 ± 0.19	0.85 ± 0.06
	global[c]		1.84 ± 0.08	0.91 ± 0.02
	anisotropy	2.23	1.76 ± 0.05	0.89 ± 0.02
L39E TR[d]			2.37 ± 0.15	0.86 ± 0.04

[a] Conditions: 10 mM sodium phosphate, 0.1 mM Na_2EDTA, pH 7.6, and 25 °C. [b] Two basis vectors were required for the thermodynamic analysis. [c] Global fits are the results of the simultaneous fitting of data sets at different protein concentrations collected by both CD and FL intensity spectroscopy. Steady-state anisotropy data were not included in the global fits because the signal, unlike FL intensity and CD, is not linearly proportional to the mole fraction of the relevant species in solution. [d] Data from Shao et al. (*30*).

Trp19/L39E TR and Trp99/L39E TR, by both fluorescence and CD spectroscopy, both showed coincident sigmoidal transitions (Figures 2 and 3) whose midpoints are independent of the protein concentration (Figure 7). These results demonstrate that the unfolding of both single-tryptophan mutants is a cooperative reaction between predominantly monomeric native and unfolded forms. Therefore, a two-state unfolding model was used to fit these data sets individually and globally.

The thermodynamic parameters obtained from the individual fits for both mutant proteins are summarized in Table 3. The good agreement between these parameters justifies a global fit of all of the FL intensity and CD data for each mutant protein; the results of the global fits are also shown in Table 3. The free energy difference between folded and unfolded monomer in the absence of denaturant, $\Delta G°(H_2O)$, and the sensitivity of the unfolding transition to urea, the m value, are 1.93 ± 0.08 kcal mol^{-1} and 0.90 ± 0.02 kcal mol^{-1} M(urea)$^{-1}$, respectively, for Trp19/L39E TR, and 1.84 ± 0.08 kcal mol^{-1} and 0.91 ± 0.02 kcal mol^{-1} M(urea)$^{-1}$, respectively, for Trp99/L39E TR at pH 7.6 and 25 °C. Trp19/L39E TR and Trp99/L39E TR display similar stabilities; however, both are less stable than monomeric L39E TR, 2.37 ± 0.15 kcal mol^{-1} (*30*). Therefore, both tryptophans play a role in stabilizing the monomeric form of the repressor. It is also interesting to note that the m value for L39E TR, 0.86 ± 0.04 kcal mol^{-1} M(urea)$^{-1}$, is similar to those for the monomeric, single-tryptophan mutants and for the burst phase intermediate in WT TR, 1.0 ± 0.1 kcal mol^{-1} M(urea)$^{-1}$.

The thermodynamic parameters of each single-tryptophan mutant obtained from anisotropy are consistent with the above global fitting results from CD and FL intensity. By globally fitting the parallel and perpendicular fluorescence

intensities, the $\Delta G°(H_2O)$ and m values were found to be 1.81 ± 0.03 kcal mol^{-1} and 0.86 ± 0.02 kcal mol^{-1} M(urea)$^{-1}$, respectively, for Trp19/L39E TR, and 1.76 ± 0.05 kcal mol^{-1} and 0.89 ± 0.02 kcal mol^{-1} M(urea)$^{-1}$, respectively, for Trp99/L39E TR (Table 3). The excellent agreement with the FL intensity and CD results indicates that the loss of packing around each of the tryptophans is associated with the global loss of secondary and tertiary structure upon unfolding.

DISCUSSION

Previous studies of the monomeric form of trp repressor, L39E TR (*30*), have shown that this species closely resembles the burst phase species detected during the folding of WT TR. However, it was not determined in that study whether monomeric tryptophan repressor contains native or nonnative tertiary structure. In the present study, two single-tryptophan-containing mutants, Trp19/L39E TR and Trp99/L39E TR, were used to probe the structural and dynamic properties of the environments of these side chains in the monomeric form.

Tertiary Structure of Monomeric TR. The combined results of CD and fluorescence spectroscopic studies suggest that both Trp19 and Trp99 occupy distinct, folded environments in monomeric TR. The same far-UV ellipticities were observed for L39E TR, Trp19/L39E TR, and Trp99/L39E TR, demonstrating that the replacement of a tryptophan in either the A or the F helix by phenylalanine does not disturb the secondary structure. Intrinsic fluorescence intensity and quenching studies showed that Trp19 and Trp99 are sequestered in hydrophobic environments and are at least partially excluded from solvent. Near-UV CD data are consistent with asymmetric environments for Trp19 and Trp99, and steady-state anisotropy demonstrated that the motions of the side chains are constrained under native conditions. Finally, the observed decreases in stability induced by their replacement with phenylalanines showed that both tryptophans contribute to the stabilization of the monomeric form. It is also noteworthy that the similar m values for the urea denaturation of the burst phase intermediate in WT TR (*29*), L39E TR (*30*), Trp19/L39E TR, and Trp99/L39E TR imply that all four monomeric forms expose comparable buried surface areas upon unfolding (*41*).

Comparison of the fluorescence results from a monomeric form of TR to those for the single-tryptophan dimeric TRs show that the local environment of Trp19 in folded, monomeric TR is different from that in the dimeric form, while the local environment of Trp99 is more similar. For example, the COM fluorescence intensities of Trp19/L39E TR and Trp99/L39E TR are red-shifted relative to that of dimeric W99F TR but are similar to that of dimeric W19F TR (Table 1). Given that Trp19 is buried in the hydrophobic core of the dimer (solvent accessible surface area of 9 Å^2) and Trp99 is only partially buried between helix F and the core (solvent accessible surface area of 35 Å^2, refs *28*, *42*), these results imply that both tryptophans in monomeric TR are only partially buried in hydrophobic environments. This conclusion is supported by the Stern−Volmer analysis (Table 2) which shows that Trp19 is somewhat more exposed to solvent than its counterpart in dimeric TR but that Trp99 has a similar exposure. In monomeric TR, the larger dynamic quenching constant for Trp99 compared to Trp19 TR further shows that Trp99 is somewhat more accessible to water-soluble quenching agents than Trp19, in agreement with the COM analysis.

The near-UV CD spectra of Trp19/L39E and Trp99/L39E TR provide further insight into the packing environments of the aromatic chromophores. The contrast between the negative signals from Trp19 near 295 nm and the positive signals from Trp99 indicate that the local environments of these chromophores are quite different from each other in monomeric TR (Figure 4). Dramatic differences are also observed between the signals from each of these side chains and their counterparts in dimeric TR. These data make it possible to conclude that both tryptophans occupy unique, well-structured environments in monomeric TR and that these environments are distinctly different from those found in the dimeric form of this protein.

The issue arises as to whether the spectroscopic differences observed between the monomeric and dimeric forms of TR simply reflect the absence of the partner subunit, rather than nonnative environments as concluded above. Inspection of the X-ray structure (Figure 1) shows that the principal contact surface for both tryptophans is provided by the other subunit. In the absence of the partner subunit and with no change in the three-dimensional structure, the solvent exposed surface area would exceed 137 Å^2 for both tryptophans. This value is substantially greater than that suggested by comparison with the quenching observed for the two tryptophans in folded, dimeric TR (Table 2), implying that a hydrophobic collapse has occurred. Such a collapse would also serve to bury many other nonpolar side chains in intramolecular, hydrophobic contacts. Therefore, it is reasonable to conclude that both Trp19 and Trp99 occupy nonnative environments in monomeric TR.

On- versus Off-Pathway Intermediate. A central question regarding the role of any transient folding intermediate is whether the species is on or off the pathway leading to the native conformation (*43*). This question can be framed in mechanistic terms for the tryptophan repressor, based upon previous studies of its folding mechanism (*29*, *44*, *45*). A simplified version of the mechanism involves only the unfolded, monomeric species, U, the folded, monomeric intermediate, I, and the native, dimeric form, N_2. For an on-pathway intermediate, the mechanism can be written as

$$2U \rightleftharpoons 2I \rightleftharpoons N_2$$

and for an off-pathway intermediate as

$$2I \rightleftharpoons 2U \rightleftharpoons N_2$$

If the on-pathway mechanism is correct, the apparent association rate constant should be decreased if the intermediate is destabilized. If the off-pathway mechanism is correct, the apparent association rate constant should be increased if the intermediate is destabilized.

The close correspondence between the transient, monomeric intermediate, I, and the stable, monomeric species, L39E TR (*30*), provides a means of eliminating the incorrect model. As demonstrated in the present study, the replacement of either Trp19 or Trp99 with phenylalanine destabilizes the monomer by approximately 0.5 kcal mol^{-1}. Previously, it has been observed that the W19F mutation

slows all three bimolecular folding phases under conditions where the association reactions in three parallel channels are rate limiting (Figure 4 in Mann et al., ref 42); the W99F mutation slows the association reactions in two of the three channels (Figure 5 in Mann et al., ref 42). Based upon these results, it appears that folded, monomeric TR is on the pathway for folding to the native dimer. Further mutational analyses are required to test the validity of this conclusion.

Hierarchical versus Nonhierarchical Folding Mechanisms. The tentative conclusion that the nonnative, monomeric burst phase intermediate for trp repressor is on the folding pathway implies that the folding does not follow a simple, hierarchical model involving the progressive development of native structure (*46*, *47*). This finding is similar to those for several other proteins whose folding mechanisms have been demonstrated (*23*, *24*, *26*, *48*) or postulated (*25*) to involve nonnative forms. Therefore, it is not uncommon for a polypeptide to form substructures that have marginal stability and that do not appear in the final, native conformation. Although these substructures must eventually undergo rearrangement reactions that may be rate limiting, it appears that the protein folding process as a whole can be enhanced by the presence of these nonnative species.

Nonhierarchical folding mechanisms may reflect the early dominance of local interactions which are ultimately superseded by nonlocal interactions that appear in later, rate-limiting steps of the reaction. Although the nonlocal interactions for many proteins serve to reinforce the locally determined structures, trp repressor is an example of another class of proteins for which the globally determined structure is very different.

ACKNOWLEDGMENT

We thank Drs. Jill Zitzewitz and Lisa Gloss for critical reviews of the manuscript and many helpful comments. We are grateful to Drs. Osman Bilsel and David Lambright for the development of in-house global fitting software.

REFERENCES

1. Dobson, C. M. (1991) *Curr. Opin. Struct. Biol. 1*, 22−27.
2. Engelhard, M., and Evans, P. A. (1995) *Protein Sci. 4*, 1553−1562.
3. Kim, P. S., and Baldwin, R. L. (1982) *Annu. Rev. Biochem. 51*, 459−489.
4. Kim, P. S., and Baldwin, R. L. (1990) *Annu. Rev. Biochem. 59*, 631−660.
5. Creighton, T. E. (1992) *Protein Folding*, W. H. Freeman and Company, New York.
6. Englander, S. W., and Mayne, L. (1992) *Annu. Rev. Biophys. Biomol. Struct. 21*, 243−265.
7. Baldwin, R. L. (1993) *Curr. Opin. Struct. Biol. 3*, 84−91.
8. Matthews, C. R. (1993) *Annu. Rev. Biochem. 62*, 653−683.
9. Bai, Y., Sosnick, T., Mayne, L., and Englander, S. (1995) *Science 269*, 192−197.
10. Balbach, J., Forge, V., Van Nuland, N. A. J., Winder, S. L., Hore, P. J., and Dobson, C. M. (1995) *Nat. Struct. Biol. 2*, 865−870.
11. Kuwajima, K. (1996) *FASEB J. 10*, 102−109.
12. Radford, S. E., Dobson, C. M., and Evans, P. A. (1992) *Nature 358*, 302−307.
13. Hooke, S. D., Radford, S. E., and Dobson, C. M. (1994) *Biochemistry 33*, 5867−5876.
14. Roder, H., Elove, G. A., and Englander, S. W. (1988) *Nature 335*, 700−704.
15. Sosnick, T. R., Mayne, L., and Englander, S. W. (1996) *Proteins 24*, 413−426.
16. Jennings, P. A., and Wright, P. E. (1993) *Science 262*, 892−896.
17. Loh, S. N., Kay, M. S., and Baldwin, R. L. (1995) *Proc. Natl. Acad. Sci. U.S.A. 92*, 5446−5450.
18. Jones, B. E., Beechem, J. M., and Matthews, C. R. (1995) *Biochemistry 34*, 1867−1877.
19. Raschke, T. M., and Marqusee, S. (1997) *Nat. Struct. Biol. 4*, 298−304.
20. Ptitsyn, O. B. (1973) *Dokl. Akad. Nauk. SSSR 210*, 1213−1215.
21. Oas, T. G., and Kim, P. S. (1988) *Nature 336*, 42−48.
22. Dill, K. A. (1990) *Biochemistry 29*, 7133−7155.
23. Hamada, D., Segawa, S., and Goto, Y. (1996) *Nat. Struct. Biol. 3*, 1−6.
24. Shiraki, K., Nishikawa, K., and Goto, Y. (1995) *J. Mol. Biol. 245*, 180−194.
25. Mok, Y.-K., Bycroft, M., and de Prat-Gay, G. (1996) *Nat. Struct. Biol. 3*, 711−717.
26. Planchenault, T., Navon, A., Schulze, A. J., and Goldberg, M. E. (1996) *Eur. J. Biochem. 240*, 615−621.
27. Vanhove, M., Lejeune, A., Guillaume, G., Virden, R., Pain, R. H., Schmid, F. X., and Frere, J.-M. (1998) *Biochemistry 37*, 1941−1950.
28. Zhang, R.-G., Joachimiak, A., Lawson, C. L., Schevitz, R. W., Otwinowski, Z., and Sigler, P. B. (1987) *Nature 327*, 591−597.
29. Mann, C. J., and Matthews, C. R. (1993) *Biochemistry 32*, 5282−5290.
30. Shao, X., Hensley, P., and Matthews, C. R. (1997) *Biochemistry 36*, 9941−9949.
31. Dulau, L., Cheyrou, A., and Aigle, M. (1989) *Nucleic Acids Res. 17*, 2873.
32. Landt, O., Grunert, H.-P., and Hahn, U. (1990) *Gene 96*, 125−128.
33. Gill, S. C., and von Hippel, P. H. (1989) *Anal. Biochem. 182*, 319−326.
34. Golub, G., and VanLoan, C. (1983) *Matrix Computations*, Johns Hopkins University Press, Baltimore.
35. Henry, E. R., and Hofrichter, J. (1992) *Methods Enzymol. 210*, 129−193.
36. Pace, C. N., Shirley, B. A., and Thomson, J. A. (1990) in *Protein Structure: A Practical Approach* (Creighton, T. E., Ed.) pp 311−330, IRL Press, New York.
37. Knutson, J. R., Beechem, J. M., and Brand, L. (1983) *Chem. Phys. Lett. 102*, 501−507.
38. Santoro, M. M., and Bolen, D. W. (1988) *Biochemistry 27*, 8063−8068.
39. Eftink, M. R., Ramsay, G. D., Burns, L., Maki, A. H., Mann, C. J., Matthews, C. R., and Ghiron, C. A. (1993) *Biochemistry 32*, 9189−9198.
40. Eftink, M. R., and Ghiron, C. A. (1976) *Biochemistry 15*, 672−680.
41. Myers, J. K., Pace, C. N., and Scholtz, J. M. (1995) *Protein Sci. 4*, 2138−2148.
42. Mann, C. J., Royer, C. A., and Matthews, C. R. (1993) *Protein Sci. 2*, 1853−1861.
43. Baldwin, R. L. (1996) *Folding Des. 1*, R1−R8.
44. Gittelman, M. S., and Matthews, C. R. (1990) *Biochemistry 29*, 7011−7020.
45. Mann, C. J., Xiao, S., and Matthews, C. R. (1995) *Biochemistry 34*, 14573−14580.
46. Kolinski, A., and Skolnick, J. (1994) *Proteins 18*, 338−352.
47. Kolinski, A., and Skolnick, J. (1994) *Proteins 18*, 353−366.
48. Kuwajima, K., Yamaya, H., and Sugai, S. (1996) *J. Mol. Biol. 264*, 806−822.
49. Kraulis, P. J. (1991) *J. Appl. Crystallogr. 24*, 946−950.

BI973171Y